ACS OMEGA

Article

Cite This: ACS Omega 2019, 4, 17634−17648

http://pubs.acs.org/journal/acsodf

Delineating the Biofilm Inhibition Mechanisms of Phenolic and Aldehydic Terpenes against *Cryptococcus neoformans*

Poonam Kumari, Neha Arora, Apurva Chatrath, Rashmi Gangwar, Vikas Pruthi, Krishna Mohan Poluri,* and Ramasare Prasad*

Department of Biotechnology, Indian Institute of Technology Roorkee, Roorkee 247677, Uttarakhand, India

Supporting Information

ABSTRACT: The recalcitrant biofilm formed by fungus *Cryptococcus neoformans* is a life-threatening pathogenic condition responsible for further intensifying cryptococcosis. Considering the enhanced biofilm resistance and toxicity of synthetic antifungal drugs, the search for efficient, nontoxic, and cost-effective natural therapeutics has received a major boost. Phenolic (thymol and carvacrol) and aldehydic (citral) terpenes are natural and safe alternatives capable of efficient microbial biofilm inhibition. However, the biofilm inhibition mechanism of these terpenes still remains unclear. In this study, we adopted an integrative biophysical and biochemical approach to elucidate the hierarchy of their action against *C. neoformans* biofilm cells. The microscopic analysis revealed disruption of the biofilm cell surface with elevation in surface roughness and reduction in cell height. Although all terpenes acted through ergosterol biosynthesis inhibition, the phenolic terpenes also selectively interacted via ergosterol binding. Further, the alterations in the fatty acid profile in response to terpenes attenuated the cell membrane fluidity with enhanced permeability, resulting in pore formation and efflux of the K^+/intracellular content. Additionally, mitochondrial depolarization caused higher levels of reactive oxygen species, which led to increased lipid peroxidation and activation of the antioxidant defense system. Indeed, the oxidative stress caused a significant decline in the amount of extracellular polymeric matrix and capsule sugars (mannose, xylose, and glucuronic acid), leading to a reduced capsule size and an overall negative charge on the cell surface. This comprehensive data revealed the mechanistic insights into the mode of action of terpenes on biofilm inhibition, which could be exploited for formulating novel anti-biofilm agents.

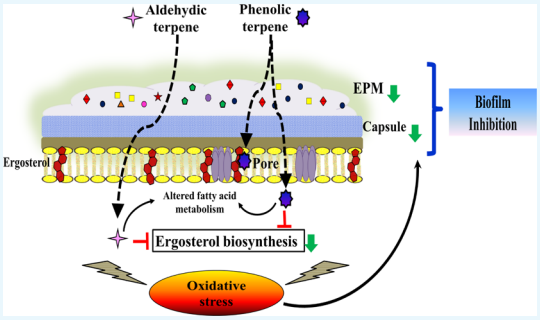

1. INTRODUCTION

Cryptococcosis is a multifaceted and potentially fatal systemic fungal infection entailing a global burden of ∼223 000 clinical cases with ∼181 100 losses inclusive of 15% AIDS-related deaths per annum.[1] *Cryptococcus neoformans*, an encapsulated yeast, is the causative agent of this systemic infection affecting lungs, skin, and the central nervous system (CNS).[2] The most acute manifestation of cryptococcal infection is meningoencephalitis, which is further challenged due to the colonization of *C. neoformans* inside the CNS to form biofilm-like cryptococcomas.[3] Moreover, the increased use of ventricular shunts for intracranial hypertension management has been associated with adherence of *C. neoformans* on these medical devices.[4,5] This highlights the significance of *C. neoformans* biofilm as a critical pathogenic condition. The biofilm is a well-structured phenotype of sessile cryptococcal cells embedded within a self-produced polysaccharide-rich extracellular polymeric matrix (EPM) attached to the surface.[3] The EPM provides mechanical stability and strong cell−cell communication and serves as a nutrient source for the biofilms.[6] It is further responsible for the recalcitrant and invasive nature of the biofilms.[3] The pathogenesis and biofilm-forming ability of *C. neoformans* is attributed to a key constituent of its polysaccharide capsule, glucuronoxylomannan (GXM).[7] The capsule of this fungal pathogen is a vital component for its survival inside the host immune system.[8] The capsular GXM aggregation forms the major part of EPM in the biofilm and is responsible for its resistance against standard antifungals.[7]

Currently, the treatment strategy for cryptococcosis comprises three main categories of antifungal agents including polyenes (amphotericin B, AMB; nystatin, NYS), azoles (fluconazole, FLC), and pyrimidine analogue (flucytosine, 5-FC).[9] However, the efficacy of these drugs against *C. neoformans* biofilms is limited. Though the biofilm forms are susceptible to AMB and its lipid formulations, the effective concentrations exceed the therapeutic range (0.025−2 μg/mL), leading to severe nephrotoxicity and emergence of drug resistance in clinical strains.[10] Cryptococcal biofilm is highly tolerant to azole group antimycotics and cannot inhibit biofilm formation as these drugs are unable to prevent GXM release, a crucial step in yeast adhesion and subsequent biofilm formation.[11] Contrary to this, *Candida albicans* biofilms are resistant to FLC owing to the presence of β-1,3-glucan, a basic component of its EPM. β-1,3-Glucan acts as a drug sponge by

Received: May 21, 2019
Accepted: September 25, 2019
Published: October 15, 2019

DOI: 10.1021/acsomega.9b01482
ACS Omega 2019, 4, 17634−17648

sequestering FLC and thereby preventing it from reaching the biofilm cell target.[12] Thus, the incompetency of these standard antifungal drugs in effectively curing biofilm-associated infections necessitates for the next stage of treatment, which is often restricted to device replacement. This incurs not only heavy cost and pain due to surgical procedure but also is further challenged by the development of resistance.[13]

Therefore, the present scenario has urged an imperative need to develop alternative natural drug therapies that are not only effective against *C. neoformans* biofilms but also safe and cost-effective. In this regard, essential oils and its active components (EO-ACs) are one of the potential drug therapies which are produced as secondary metabolites by the aromatic plants. These are complex and volatile compounds with well-established antimicrobial and antibiofilm potential against different pathogens.[14,15] Among the EO-ACs, thymol (THY), carvacrol (CARV), and citral (CIT) have been extensively reported to strongly inhibit biofilms of pathogenic bacteria including carbapenemase-producing Gram-negative bacilli, uropathogenic *Escherichia coli,* and fungilike *C. albicans* and *Cryptococcus* spp (Figure 1).[16,17] Both THY and CARV are

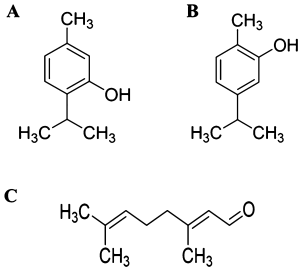

Figure 1. Chemical structure of phenolic terpenes (A) THY and (B) CARV and aldehydic terpene (C) CIT. Chemical structures were drawn using ChemDraw software.

phenolic terpenes obtained from *Thymus vulgaris* and *Origanum vulgare,* whereas CIT is an aldehydic terpene extracted from *Cymbopogon citratus.* A few studies have explored the plausible mode of action of THY, CARV, and CIT against planktonic form of various microorganisms including *Staphylococcus aureus, Pseudomonas aeruginosa, Cronobacter sakazakii, Mycobacterium avium, Candida* sp., *Aspergillus flavus,* and so forth.[18,19] However, till date, no detailed reports are available on the mechanism of biofilm inhibition/eradication.

In a recent study, our group analyzed the anti-biofilm activity of THY, CARV, and CIT against *C. neoformans* and their nontoxicity toward human cell lines.[17] In order to comprehend their mode of action against the biofilm, holistic insight into the phenotypic and physiological alterations is quintessential. Hence, the present study focuses on delineating the biofilm inhibition mechanism of the terpenes (THY, CARV, and CIT) by analyzing the morphological changes and qualitative/quantitative alterations in the EPM and cellular components of *C. neoformans* biofilm cells.

2. RESULTS

2.1. Assessing the Changes in the Surface Topography of *C. neoformans* Biofilm Cells. The surface topographical analysis of the cell's outer surface is a noteworthy indicator of its health state. The surface topography of biofilm cells treated at 0.5× or 1/2 BIC_{80} of THY (16 μg/mL), CARV (32 μg/mL), and CIT (64 μg/mL) (Table S1 in the Supporting Information) was visualized on both micro and nanoscale levels using field emission scanning electron microscopy (FE-SEM) and atomic force microscopy (AFM), respectively. The FE-SEM/AFM micrographs of the control (CK) biofilm cells showed a spherical and turgid cellular morphology with a smooth and uniform topography throughout the surface (Figure 2A, panels I, II). In contrast, the terpene(s)-treated biofilm cells indicated severe damage and shrunken morphology with aberration on the cellular surface resulting in pores along with the rupturing of the cells (Figure 2A, panels I, II). These results are in correlation with the alterations reported in the *C. albicans* biofilm cells after treatment with *C. citratus* EOs.[20]

Additionally, to get quantitative insights into changes in surface topography, three-dimensional based high spatial resolution AFM analysis was performed. The CK biofilm cells appeared normal in morphology with a smooth outer surface. On the contrary, THY- and CAR- treated cells exhibited collapsed margins with a convoluted and bumpy surface, and CIT-treated cell surfaces were relatively less damaged with the presence of a few septa (Figure 2A, panel III). The above visual morphological alterations were also supported by significant variations in the biophysical properties, particularly surface roughness and cell height of *C. neoformans* (Figure 2B,C). The biofilm cells treated with THY (∼918 nm), CAR (∼1005 nm), and CIT (∼1186 nm) showed a significant reduction in cell height in comparison to CK (∼1588 nm), as shown in Figure 2B. Furthermore, the root−mean-square of surface roughness remarkably increased in treated biofilm cells because of membrane shrinkage caused by the terpenes (Figure 2C).

2.2. Determining the Qualitative and Quantitative Changes in the EPM. Fourier transform infrared spectroscopy (FT-IR) provides a first line of evidence regarding the compositional analysis of biomolecules present in a given sample. The FT-IR spectra of CK and terpene-treated biofilm EPM showed the presence of polysaccharides (1300−900 cm^{-1}) and proteins (1700−1500 cm^{-1}).[21] The most remarkable spectral differences between CK and treated EPM was noticed in the range of 900−1200 cm^{-1}, representing the variable interactions at carbonyl (C═O) moieties present in the polysaccharides. The peak at 982 cm^{-1} in CK shifted to 1021 cm^{-1} in the case of CIT, suggesting its interaction with C−O−C and C−O−P rings present in the polysaccharides. On the other hand, the above peak completely disappeared in THY- and CARV-treated EPM (Figure 3A). Further, the absorption peaks at 1569 cm^{-1} in CK EPM shifted to 1579 cm^{-1} (THY), 1580 cm^{-1} (CARV), and 1583 cm^{-1} (CIT), indicating a stronger interaction of the above terpenes with N−H and C−N in the peptide backbone of the amide II region (Figure 3A). The peak intensities for polysaccharides and proteins were observed to be higher in CK EPM as compared to terpene-treated samples (Figure 3A). The above results were corroborated by performing the quantitative analysis. The EPM of CK samples accounted for ∼90% of total carbohydrate with only ∼5% total protein (Figures 3B and S1). On the other hand, the terpene-treated samples showed a significant reduction (35−45%) in total carbohydrates, whereas no noticeable changes were recorded in the total protein content (Figures 3B and S1).

2.2.1. Evaluating the Alterations in the Glycosyl Composition of EPM. The changes in the carbohydrate

DOI: 10.1021/acsomega.9b01482
ACS Omega 2019, 4, 17634−17648

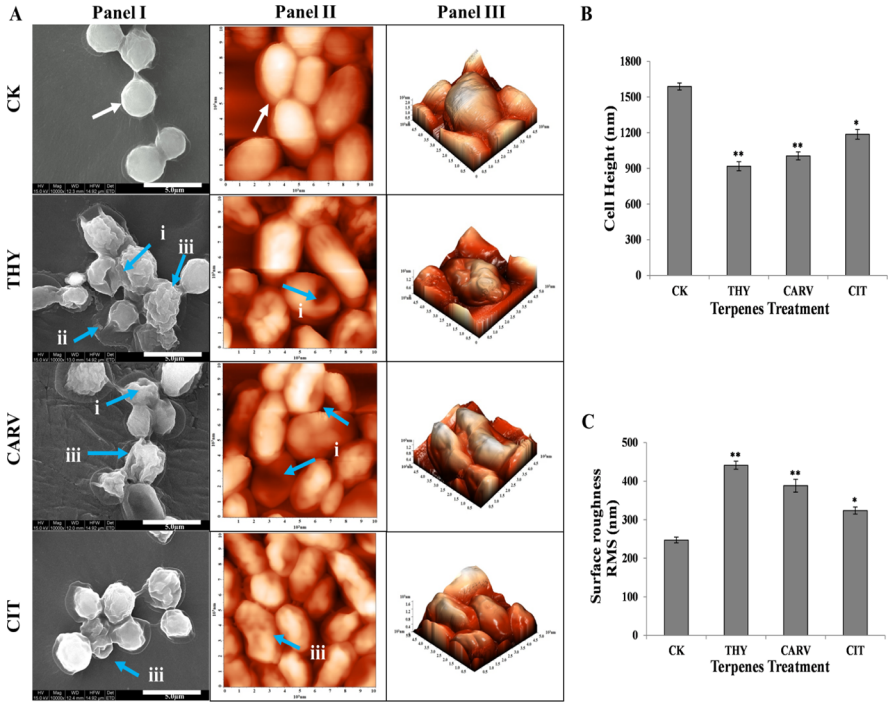

Figure 2. *C. neoformans* biofilm cell surface morphology and biophysical parameters: (A) Field emission scanning electron micrographs (panel I) and atomic force micrographs showing two- and three-dimensional view of the cell surface ultrastructure (panels II, III); white arrow indicates a turgid cellular morphology with a smooth surface topography while blue arrows (i) show surface aberration in the form of pores; (ii) burst cells with oozing contents; and (iii) wrinkled outer surface. (B) Cell height and (C) surface roughness before (control; CK) and after treatment with 1/2 BIC_{80} of THY (16 μg/mL), CARV (32 μg/mL), and CIT (64 μg/mL) for 6 h. Results represent average ± SD (n = 3) and *p < 0.05, **p < 0.001 when compared with CK.

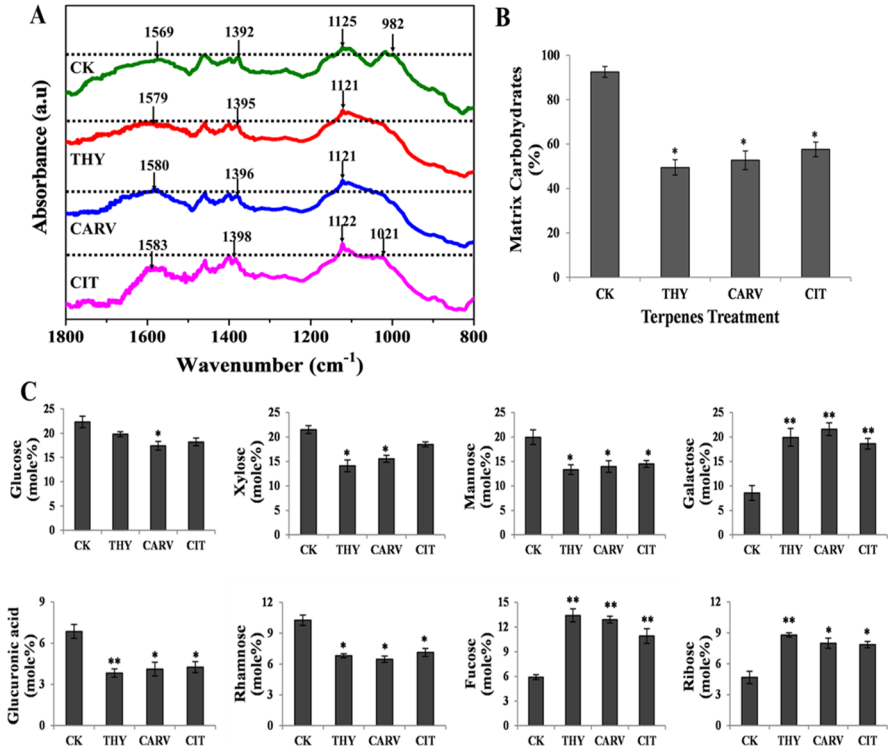

Figure 3. Analysis of EPM: (A) FT-IR; (B) carbohydrates % and (C) glycosyl composition of EPM before (control; CK) and after phenolic/aldehydic terpene treatment at 1/2 BIC_{80} (THY-16 μg/mL, CARV-32 μg/mL, and CIT-64 μg/mL) for 6 h. Values are represented as mole % of total carbohydrate in EPM. The data represents average ± SD (n = 3) and *p < 0.05, **p < 0.01 when compared with CK.

glycosyl composition were determined by calculating the mole % amount of individual glycosyl residues in the EPM. The carbohydrates in the EPM of CK biofilm majorly comprised of glucose, xylose, and mannose amounting to ∼64% of the total

DOI: 10.1021/acsomega.9b01482
ACS Omega 2019, 4, 17634−17648

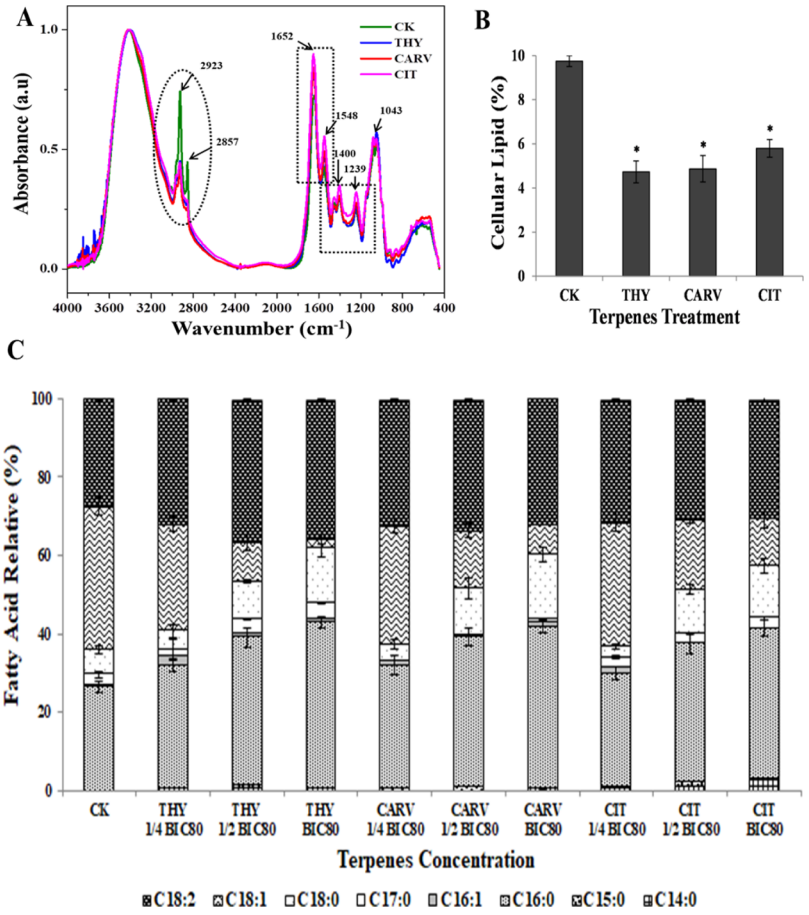

Figure 4. Cellular macromolecules composition analysis: (A) FT-IR; (B) lipid % and (C) FAME composition before (control; CK) and after phenolic/aldehydic terpene treatment at 1/2 BIC_{80} (THY-16 μg/mL, CARV-32 μg/mL, and CIT-64 μg/mL) for 6 h. The data represents average ± SD (n = 3) and *p < 0.05 when compared with CK.

carbohydrate, while rhamnose, galactose, glucuronic acid, ribose, and fucose formed the rest (~36%) (Figure 3C). The carbohydrate content in terpene-treated EPM showed variation in the amount of glycosyl residues (Figure 3C). All terpene-treated EPM displayed a significant reduction in glucuronic acid, mannose, and rhamnose contents; however, the decrease in the content of sugars such as glucose and xylose were differential in the terpene-treated samples. Interestingly, the amount of galactose, fucose, and ribose significantly increased in all treated EPMs, suggesting perturbation in the matrix structure of the treated biofilm (Figure 3C).

2.3. Determining the Qualitative and Quantitative Changes in the Cellular Macromolecules. FT-IR spectroscopy was conducted to identify the changes in the principal biological components of the biofilm cells after respective terpene treatment. To elucidate the changes in the biomolecular composition, FT-IR spectra has been divided into five regions: lipids (3000−2800 cm^{-1}), proteins/amides I, II (1700−1500 cm^{-1}), phospholipids/nucleic acids (1500−1200 cm^{-1}), polysaccharides (1200−900 cm^{-1}), and the fingerprint region (900−600 cm^{-1}).[21] The spectra region between 1700−1500, 1500−1200, 900 and 1200 cm^{-1} exhibited no distinctive variations in spectral properties, indicating that terpenes did not affect the proteins, DNA/RNA, and polysaccharides in the biofilm cells (Figure 4A, black dotted rectangles). The biochemical assay results on these biomolecules also evidenced no significant change, thus substantiating the infrared spectroscopy results (Figures S2 and S3). The most striking difference was observed in the spectral range of 3000 and 2800 cm^{-1}, signifying that membrane fatty acids were majorly affected by terpene treatment (Figure 4A, black dotted oval). The reduced peak intensity at 2923 cm^{-1} which conform to the asymmetric ν_{as} (CH_2) stretching in fatty acids was observed in the treated cells, suggesting molecular interaction of the terpenes with fatty acids and in-turn reduced membrane fluidity. Further, a peak at 2857 cm^{-1} attributed to symmetric ν_s (CH_2) stretching of $>CH_2$ functional groups in fatty acids completely disappeared under treatment conditions, indicating structural changes.[22] The FT-IR results were further supported by a quantitative analysis which showed remarkable differences in the lipid content of terpene-treated biofilm cells as compared to CK (Figure 4B). The lipid content in THY-, CARV-, and CIT-treated biofilm cells were reduced by ~52, ~50, and ~41%, respectively (Figure 4B).

2.3.1. Analyzing the Fatty Acid Profile Changes. The fatty acid compositional analysis can potentially shed light on how the constituents of fatty acids modulate the permeability and fluidity of the cell membranes under differential stress conditions.[23] To delineate such changes, the fatty acid composition of *C. neoformans* biofilm cells without treatment (CK) and with THY (8, 16, 32 μg/mL), CAR (16, 32, 64 μg/mL), and CIT (32, 64, 128 μg/mL) treatments at 0.25× or 1/4 BIC_{80}, 0.5× or 1/2 BIC_{80}, and 1× BIC_{80}, respectively, were

DOI: 10.1021/acsomega.9b01482
ACS Omega 2019, 4, 17634−17648

determined (Figure 4C and Table S2). The major composition of the fatty acids in *C. neoformans* includes palmitic acid (C16:0), hexadecanoic acid (C17:0), stearic acid (C18:0), oleic acid (C18:1), and linoleic acid (C18:2). After 6 h incubation with the terpenes, no significant changes were observed at 0.25× or 1/4 BIC_{80}, while moderate changes were noted at 0.5× or 1/2 BIC_{80}, and the most prominent changes in the fatty acid profile were observed at 1× BIC_{80} (Figure 4C). Among the saturated fatty acids (SFAs), the relative quantity of palmitic acid increased from ∼26% (CK) to ∼43% (THY), ∼41% (CARV), and ∼39% (CIT), respectively, at 1× BIC_{80} treatment with $p < 0.01$. However, the amount of hexadecanoic acid augmented from ∼2.9 to ∼4.2% in the case of THY, whereas CARV and CIT treatments resulted in ∼1.2 and ∼2.7% reduction, respectively (Figure 4C). Additionally, the relative amount of stearic acid increased by more than 2-fold from ∼6.3% (CK) to ∼14.1% (THY), ∼16.5% (CARV), and ∼13.2% (CIT). Among the terpenes, THY caused maximum increase in the proportions of SFAs, followed by CARV and CIT (Table S2). In the case of unsaturated fatty acids (UFAs), particularly, the oleic acid content decreased to ∼2.4, ∼7.8, and ∼12.3% in THY, CARV, and CIT, respectively, in comparison to CK (∼36.65%) at 1× BIC_{80} treatment. However, the relative amount of linoleic acid was enhanced from ∼27.7 to ∼35.59% (THY), ∼33.06% (CARV), and ∼30.41% (CIT) as depicted in Figure 4C. Such changes in the individual fatty acid constituents resulted in a significant reduction of UFA/SFA ratio from 1.81 to 0.64, 0.69, and 0.75 at BIC_{80} treatment of THY, CAR, and CIT, respectively, which could essentially influence the cell fluidity. It is clear from the results that the terpenes caused an adverse effect on the total lipid profile of *C. neoformans* biofilm cells.

2.4. Evaluating the Effect of Terpenes on the Cell Wall and Capsule. The presence of a capsule on the cell wall is one of the unique features of *C. neoformans*. Hence, the effect of the terpenes on cell wall binding and different capsule features such as size and surface charge was analyzed.

2.4.1. Sorbitol Assay. Sorbitol assay evaluates the role of the cell wall in the antifungal mechanism of terpenes. Sorbitol is an osmoprotectant that stabilizes the cell wall under stress. In general, an increase in MIC_{80}/BIC_{80} will be observed in the sorbitol presence if the mode of action of the drug is through direct attachment to the cell wall. The MIC_{80} and BIC_{80} values for the terpenes against *C. neoformans* did not alter in the presence of osmotic protector sorbitol, indicating that the antifungal action of THY, CARV, and CIT did not affect the cell wall integrity directly (Table 1). In line with the literature, the MIC_{80} (32 μg/mL) and BIC_{80} (128 μg/mL) values for the cell wall acting drug (CASP) increased to 4-fold and 8-fold, respectively, in the presence of sorbitol.

Table 1. MIC_{80} and BIC_{80} of Terpenes and Standard Drugs against *C. neoformans* in the Presence (+) and Absence (−) of Sorbitol[a]

	(−)sorbitol		(+)sorbitol	
	MIC_{80}	$BIC_{80}^{\#}$	MIC_{80}	$BIC_{80}^{\#}$
	Terpenes			
THY	16	32	16	32
CARV	32	64	32	64
CIT	64	128	64	128
	Positive CK			
CASP	32	128	256	>1024

[a]$BIC_{80}^{\#}$ was determined by measuring XTT reduction activity.

2.4.2. Assessing the Changes in the Capsule Size and Surface Charge. In order to assess the action of terpenes on capsule properties, the changes in the capsule size and surface charge were analyzed. Indian ink-stained capsule images of terpene-treated *C. neoformans* biofilm cells indicated a reduction in size as compared to CK (Figure 5A). The capsule size of THY (1.33 μm)-, CARV (1.56 μm)-, and CIT (1.95 μm)-treated biofilm cells significantly decreased by 49%, 40%, and 25%, respectively, in comparison to CK (2.58 μm) (Figure 5B). Further, in the presence of 0.5× or 1/2 BIC_{80} of phenolic/aldehydic terpenes, a significant decline in the surface negativity of biofilm cells was observed. The surface negativity reduction was maximum in the case of THY (−2.5 *z*/mV) followed by CARV (−3.6 *z*/mV) and CIT (−5.6 *z*/mV) as shown in Figure 5C.

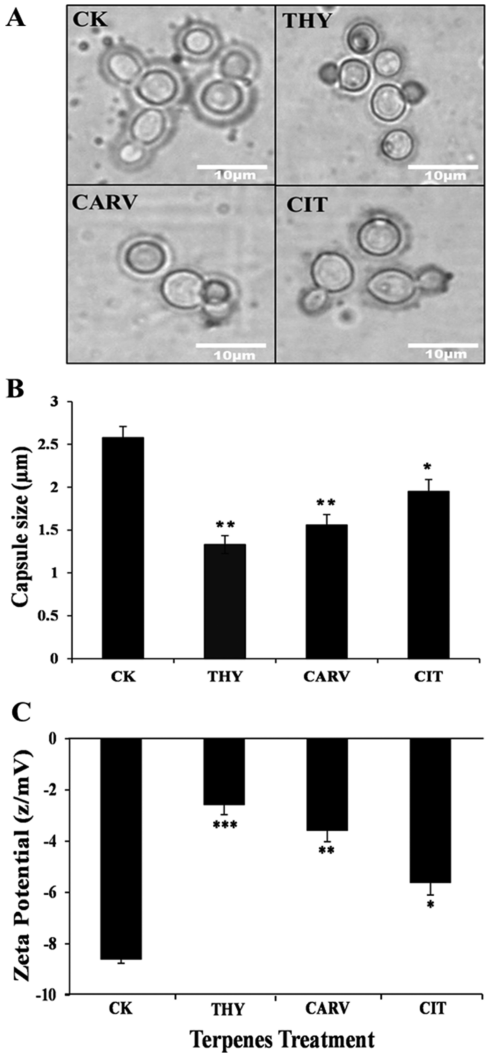

Figure 5. Alterations in the capsule size and cell surface charge: (A) Light microscopic images of Indian ink-stained cells; (B) capsule size measurement; and (C) ZP before (control; CK) and after phenolic/aldehydic terpene treatment at 1/2 BIC_{80} (THY-16 μg/mL, CARV-32 μg/mL, and CIT-64 μg/mL) for 6 h. The data represents the average ± SD ($n = 3$) and *$p < 0.05$, **$p < 0.01$, and ***$p < 0.001$ when compared with CK.

DOI: 10.1021/acsomega.9b01482
ACS Omega 2019, 4, 17634−17648

Table 2. MIC_{80} and BIC_{80} of Terpenes and Standard Drugs against *C. neoformans* in the Presence (+) and Absence (−) of Ergosterol[a]

	(−)ergosterol				(+)ergosterol			
			100 (μg/mL)		200 (μg/mL)		400 (μg/mL)	
	MIC_{80}	$BIC_{80}^{\#}$	MIC_{80}	$BIC_{80}^{\#}$	MIC_{80}	$BIC_{80}^{\#}$	MIC_{80}	$BIC_{80}^{\#}$
Terpenes								
THY	16	32	32	128	64	256	128	512
CARV	32	64	64	256	128	512	256	1024
CIT	64	128	64	128	64	128	64	128
Positive CK								
AMB	1	4	4	32	8	64	16	128
NYS	2	8	8	64	16	128	32	256

[a]$BIC_{80}^{\#}$ was determined by measuring XTT reduction activity.

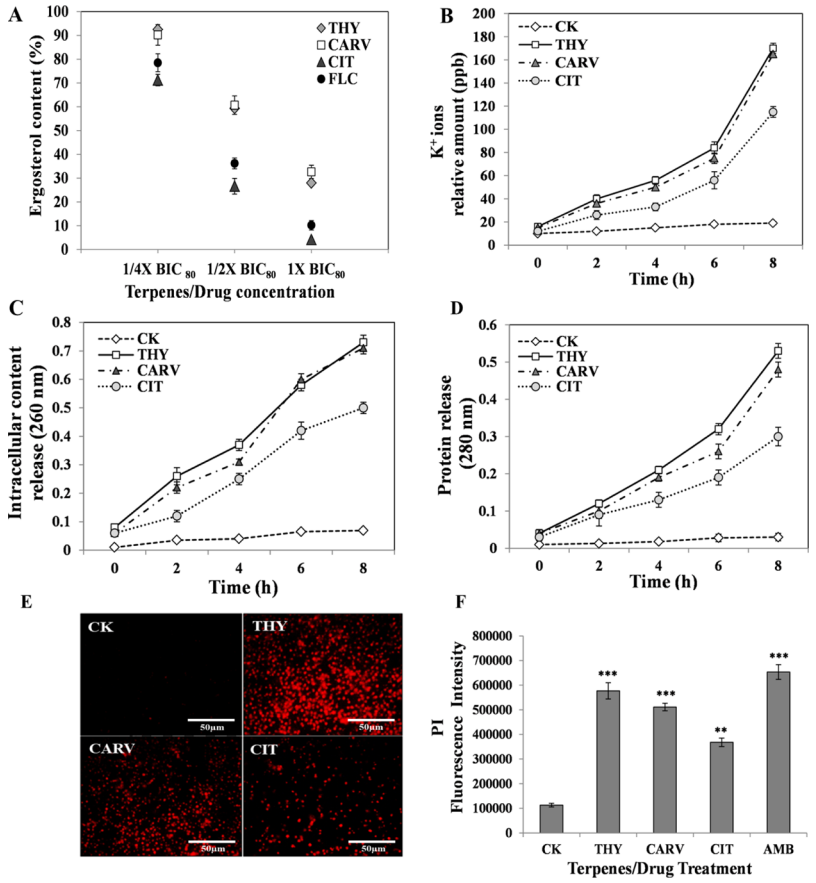

Figure 6. Modulation of membrane permeability and integrity: (A) Ergosterol content %; (B) potassium leakage; (C) intracellular content release; (D) protein release; (E) fluorescence intensity of PI; and (F) fluorescence micrographs of PI-stained cells before (control; CK) and after phenolic/aldehydic terpene treatment at 1/2 BIC_{80} (THY-16 μg/mL, CARV-32 μg/mL, and CIT-64 μg/mL). The ergosterol content in the untreated CK (control) was considered 100%. Positive control: FLC and AMB. The data represents the average ± SD (n = 3) and $^{**}p < 0.01$, $^{***}p < 0.001$ when compared with CK.

2.5. Analyzing the Changes in Membrane Permeability and Integrity. *2.5.1. Ergosterol Binding and Quantification Assay.* Ergosterol is unique to fungi and has multifacet roles involving the maintenance of membrane fluidity, integrity, and proper functioning of membrane-bound enzymes.[24] Ergosterol-binding assay was performed to investigate the possible action of phenolic/aldehydic terpenes (THY, CARV, and CIT) on the fungal cell membrane and their ability to form complexes with ergosterol. The results revealed a 2−8 fold increase in the MIC_{80} values and a 4−16 fold increase in the BIC_{80} values of THY and CARV in the presence of 100−400 μg/mL of ergosterol, thus suggesting the action of above terpenes through membrane ergosterol binding, as evident by comparison with positive control drugs (AMB, NYS). However, the MIC_{80} and BIC_{80} values of CIT did not alter, suggesting that this aldehydic terpene does not bind to ergosterol directly (Table 2).

To explore the effect of the above terpenes on the ergosterol biosynthesis level, the amount of ergosterol in biofilm cells was determined at three different concentrations (0.25× or 1/4 BIC_{80}, 0.5× or 1/2 BIC_{80}, and 1× BIC_{80}). The phenolic/aldehydic terpenes displayed a significant modulation of

DOI: 10.1021/acsomega.9b01482
ACS Omega 2019, 4, 17634−17648

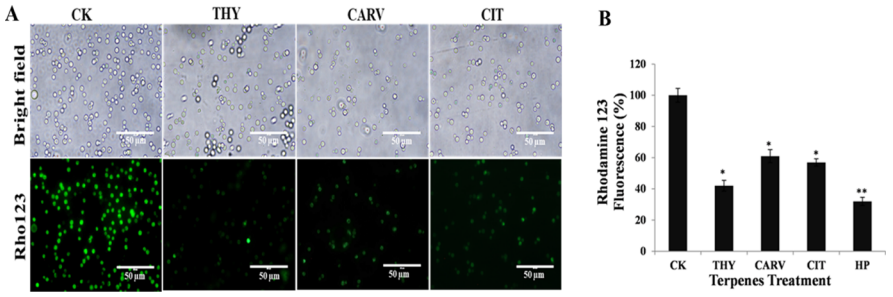

Figure 7. Evaluation of mitochondrial membrane potential ($\Delta\Psi_m$): (A) relative fluorescence intensity of Rho123 and (B) fluorescence micrographs of Rho123-stained cells before (control; CK) and after phenolic/aldehydic terpene treatment at 1/2 BIC_{80} (THY-16 μg/mL, CARV-32 μg/mL, and CIT-64 μg/mL) for 6 h. The data represents the average ± SD (n = 3) and *p < 0.05, **p < 0.01 when compared with CK.

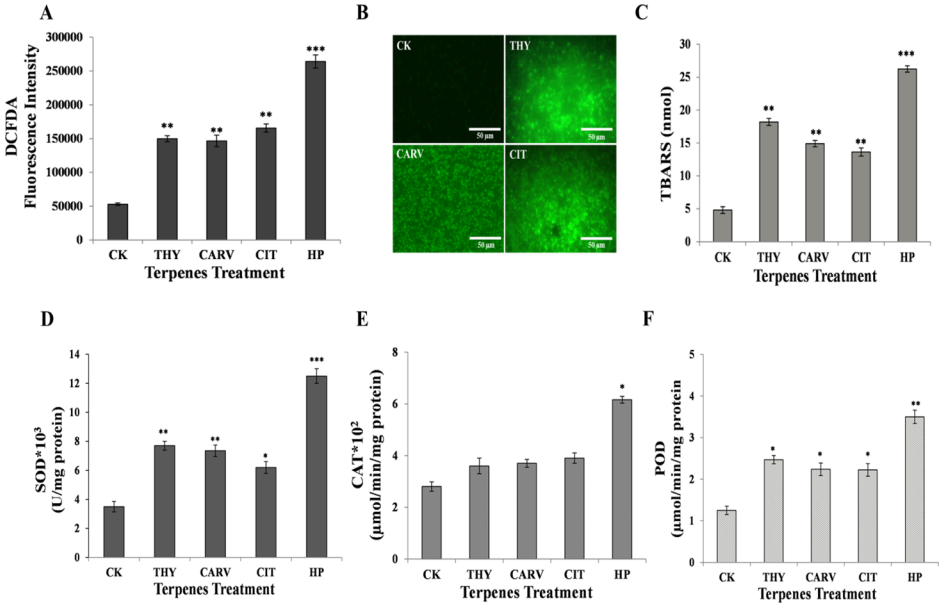

Figure 8. Elevation of oxidative stress and related antioxidant enzymes activity: (A) amount of ROS; (B) fluorescence micrographs of DCFDA-stained cells; (C) lipid peroxidation (TBARS); (D) SOD; (E) CAT; and (F) peroxidase before (control; CK) and after phenolic/aldehydic terpene treatment at 1/2 BIC_{80} (THY-16 μg/mL, CARV-32 μg/mL, and CIT-64 μg/mL) for 6 h. Positive control: HP. The data represents the average ± SD (n = 3) and *p < 0.05, **p < 0.01, and ***p < 0.001 when compared with CK.

ergosterol content in a dose-dependent manner (Figure 6A). Among the terpenes, the aldehydic terpene CIT (64 μg/mL) at 1× BIC_{80} exhibited the maximum reduction in ergosterol content, which was comparable to the positive control drug (FLC), a well-known inhibitor of ergosterol biosynthesis, suggesting that it acted by disrupting the ergosterol biosynthetic pathway (Figure 6A). On the other hand, reduction in the ergosterol content by phenolic terpenes THY (16 μg/mL) and CARV (32 μg/mL) at their respective 1× BIC_{80} was comparatively less (Figure 6A).

2.5.2. Extracellular Potassium Leakage Assay. The potassium (K^+) ion leakage from the cell to the outside environment is an indicator of disorganization of membrane permeability and integrity. To ascertain the action of phenolic/aldehydic terpenes on the biofilm cell membrane, the amount of K^+ ion leakage was evaluated. All three terpenes displayed a time-dependent rise in K^+ ion leakage in comparison to control (CK). Among the terpenes, THY induced the maximum K^+ ion leakage, closely followed by CARV (Figure 6B). Although the treatment with the aldehydic terpene CIT significantly increased the K^+ ion leakage, the amount of K^+ ions leaked was lower in comparison to both the phenolic terpenes (Figure 6B).

2.5.3. Intracellular Content and Protein Release. To study the mechanism of phenolic/aldehydic terpenes acting at the level of membrane permeability, the release of intracellular content (DNA/RNA/nucleotides) and protein from the biofilm cells was assessed (Figure 6C,D). A consistent rise in the intracellular content and protein release with time was observed in THY-, CARV-, and CIT-treated biofilm cells. The phenolic/aldehydic terpenes initiated the damage of fungal membrane within 2 h of exposure causing cytoplasmic leakage. At the 8 h time point, THY and CARV were equally effective, followed by CIT (Figure 6C). The proteins released into the supernatant were also found to be in line with the release of intracellular content (Figure 6D), indicating that prolonged exposure to the terpenes resulted in a severe membrane impairment.

2.5.4. Plasma Membrane Integrity Assay. The membrane damaging effects of phenolic/aldehydic terpenes were confirmed by the propidium iodide (PI) assay. PI is a DNA intercalating fluorescent dye employed to examine the action of drugs on the cell membranes. The maximum fluorescence of

DOI: 10.1021/acsomega.9b01482
ACS Omega 2019, 4, 17634−17648

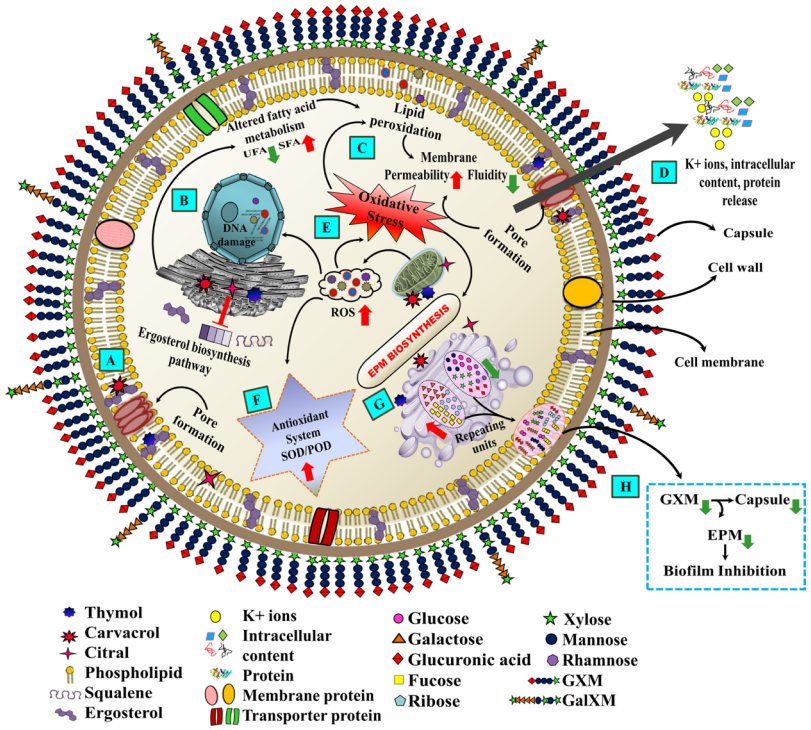

Figure 9. Schematic representation illustrating the biofilm inhibition mechanism of phenolic/aldehyde terpenes (THY, CARV, and CIT) against *C. neoformans*. (A) Entry of terpenes into the cell, (B) altered fatty acid metabolism/ergosterol biosynthesis, (C) membrane permeability/fluidity changes, (D) intracellular content and K^+ ions leakage, (E) ROS generation/oxidative stress, mitochondrial depolarization, and lipid peroxidation, (F) antioxidant defense responses, (G) altered EPM biosynthesis pathway, and (H) capsule size reduction. All of the above mechanisms lead to biofilm inhibition and cell lysis. The red arrows indicate an increase while green arrows indicate a reduction/decrease.

internalized PI was observed in THY, followed by CARV and then CIT, suggesting its strong potency against biofilm cells by causing membrane lesions, which further leads to loss of cell viability. It is worth noting that the membrane-damaging potential of phenolic terpenes is comparable to that of commercial drug AMB (Figure 6F). The above results were also supported by PI-stained fluorescence microscopic images, which exhibited enhanced red fluorescence of dead/damaged biofilm cells on terpene exposure (Figure 6E).

2.6. Evaluating the Oxidative Stress and Antioxidant Defense System Responses. *2.6.1. Assessment of the Mitochondrial Membrane Potential.* Mitochondrion is the main organelle involved in the reactive oxygen species (ROS) generation and plays a key role in oxidative stress-induced cell death.[25] The terpene treatment caused mitochondrial depolarization by significantly reducing the mitochondrial membrane potential ($\Delta\Psi_m$) in comparison to CK (Figure 7B). The relative fluorescence intensity reduced to ∼42, ∼61, and ∼57% in the case of THY-, CARV- and CIT-treated biofilm cells (Figure 7B). The rhodamine 123 (Rho123)-stained fluorescent images of biofilm cells further verified that the terpenes caused loss of $\Delta\Psi_m$ (Figure 7A).

2.6.2. ROS Quantification and Lipid Peroxidation. The phenolic/aldehydic terpenes are known to trigger the generation of ROS, which results in lipid peroxidation. The intracellular ROS levels in the terpene-treated biofilm cells was monitored by employing a specific fluorogenic probe H_2DCFDA (Figure 8A). A substantial enhancement in the fluorescence intensity was detected in the biofilm incubated with terpenes, suggesting the accumulation of ROS (Figure 8A). The enhanced ROS production in the terpene-treated cells was also evident from the fluorescence images that exhibited enhanced green fluorescence (Figure 8B).

The oxidative damage caused to membrane lipids can be estimated using lipid peroxidation byproducts, thiobarbituric acid reactive substances (TBARS). In comparison to CK, the TBARS content remarkably increased by ∼5.4, ∼3.8, ∼3.3, and ∼2.7-folds in hydrogen peroxide (HP)-, THY-, CARV-, and CIT-treated biofilms, respectively, suggesting membrane damage (Figure 8C).

2.6.3. Superoxide Dismutase, Catalase, and Peroxidase Activities. The protective response of *C. neoformans* biofilm cells to the elevated levels of free radicals/ROS was determined by assessing the modulation in the activities of the antioxidant enzymes such as superoxide dismutase (SOD), catalase (CAT), and peroxidase (POD). All three terpenes (THY, CARV, and CIT) instigated an elevation of ∼1.6−2.3-fold in the activities of SOD and POD as compared to the CK biofilm (Figure 8D,F). A profound upsurge in the SOD and POD activities of biofilm cells in response to terpenes suggested accumulation of superoxide and peroxide species. However, the terpene-treated biofilm cells did not show any significant change in the CAT activity (Figure 8E).

3. DISCUSSION

The multifactorial defense mechanism of cryptococcal biofilms confers resistance to standard antifungal treatment and is responsible for causing morbidity/mortality due to recalcitrant human infections. These mechanisms include EPM, high cell density, upregulation of efflux pumps, and persister cell population.[26] The binding and sequestration of drugs by EPM of biofilms seems to be the most universal mechanism of resistance against the standard antifungals.[27] Additionally, the

DOI: 10.1021/acsomega.9b01482
ACS Omega 2019, 4, 17634−17648

large size of synthetic drugs hinders in diffusion and penetration into the matrix of the biofilm.[28] This ultimately leads to the trapping of drugs in the carbohydrate-rich EPM turning drugs ineffective against the biofilms.[29] Thus, the current situation has put a tremendous liability on the scientific community to search and develop novel alternative agents that are small, amphipathic, and nontoxic to efficiently combat cryptococcal biofilms by diffusing/penetrating through EPM. In this regard, previous reports have established natural phenolic (THY and CARV) and aldehydic (CIT) terpenes as potential candidates against biofilms.[15−17] Recently, we reported the nontoxic behavior of these phenolic/aldehydic terpenes at their respective BIC_{80} falling into a safe dosage range without causing substantial toxicity against human keratinocytes and renal cells.[17] The phenolic terpenes THY/CARV caused ∼8−11% loss in viability of keratinocytes at 32 μg/mL. On the other hand, CIT at the similar dose affected ∼22% keratinocytes, suggesting the less toxic attribute of phenolic terpenes in comparison to aldehydic terpenes. Indeed, the coculture infection model further revealed the selective action of phenolic terpenes against cryptococcal cells without affecting keratinocytes. In line with these results, Elshafie et al. demonstrated the high toxicity of THY and CARV at 289 μg/mL against tumor cells rather than healthy renal cells.[30] The above findings undoubtedly establish these terpenes as potentially safe anti-biofilm candidates. However, a detailed mechanism of action for these natural antifungal agents against the infectious biofilm forms is not yet known. The current study adopted an integrative approach comprising morphological, biophysical, and biochemical studies to elucidate the hierarchy of their action on the cellular level.

In general, terpenes can act against the fungal biofilm at the level of the cell wall, plasma membrane, or both. The terpenes penetrate deeply into the phospholipid bilayer because of their high hydrophobic and partition coefficient values.[31] Interestingly, none of the terpenes targeted the biofilm via the cell wall, as no change in MIC_{80}/BIC_{80} was recorded in the presence of osmoprotectant sorbitol (Table 1). Among the terpenes, THY and CARV showed an increase in the BIC_{80} values upon addition of ergosterol, suggesting their first line of action via membrane ergosterol sequestration leading to pore formation (Table 2 and Figure 9; panel A). These two terpenes also significantly reduced the endogenous ergosterol, depicting their dual action on membrane ergosterol as well as its biosynthesis. On the other hand, CIT though did not involve direct interaction with membrane ergosterol, but indeed it acted via inhibition of ergosterol biosynthesis (Figures 6A and 9; panel B). Our results were corroborated by recent reports on ergosterol biosynthesis inhibition caused by CIT in planktonic forms of different fungal species.[32,33] A comparative analysis of the membrane-rupturing properties of these terpenes suggested that the phenolic terpenes (THY and CARV) were more effective than the aldehydic terpene (CIT). The presence of the hydroxyl group in phenolic terpenes enhances their hydrophilic ability, resulting in intense membrane impairment.[34]

The second line of action of terpenes could be through lipid profile alterations. It is well known that microbial cells adapt under stress via modulating their SFA to UFA content, which maintains the membrane integrity.[35] The fatty acid profile of the treated biofilm cells revealed an increase in the SFA/UFA ratio with a significant rise in the palmitic acid content. Such an increase in palmitic acid makes the cell membrane more rigid and less fluid, thereby disrupting membrane integrity through its aggregation and pore formation (Figures 4C, 9; panel C, and Table S2).[36] The PI incorporation into the biofilm cells confirmed the increased permeability and irreversible perturbations of membrane integrity caused by the terpenes (Figure 6E,F).[33] The above findings corroborated with previous studies on planktonic forms of *Listeria monocytogenes*, *Pseudomonas fluorescens*, *S. aureus*, *Shewanella putrifaciens*, and *C. albicans* treated with different EOs and EO-ACs.[23,35,37,38] Such pore formation results in the damage of cell membrane and consequent efflux of intracellular contents including K^+ ions, nucleotides/DNA/RNA, and protein (Figures 6B−D and 9; panel D).

The dysregulation of ion homeostasis because of K^+ efflux and depolarization of mitochondrial membrane triggers ROS generation, resulting in oxidative stress which could be the third line of action of these terpenes against biofilm cells (Figures 7, 8A, and 9; panel E).[39,40] In line with our results, recent studies have validated the antimicrobial action of a few terpenes, which were positively related to the ROS accumulation.[41,42] The undesirable accumulation of ROS not only disrupts organelle-like mitochondria or plasma membrane but also causes oxidative damage to biological macromolecules.[43] The elevated levels of TBARS in synergy with reduced ergosterol content in biofilm cells elicited severe oxidative degradation of membrane lipids (Figures 8C and 6A). The antioxidant enzymes were also activated in biofilm cells as a protective response against enhanced ROS levels to limit cell damage (Figures 8 and 9; panel F). Indeed, the extent of oxidative stress and cell survival fate is regulated by the equilibrium between ROS generation and antioxidant defenses.[44]

The enhanced ROS accumulation and oxidative stress can also attenuate the biosynthesis of the capsule.[45] The capsule GXM forms the major portion of EPM composition, which plays a crucial role in the resistance against antifungal drugs.[26] A significant reduction in the capsule size and total carbohydrate content of EPM after terpene treatment indicates their final line of action (Figures 3B and 9; panel G). Recently, Panariello et al. reported a similar reduction in alkali and water-soluble polysaccharides of FLC susceptible *Candida* sp. EPM.[46] The release of capsular polysaccharide on to the external surface to form EPM is essential for *C. neoformans* adhesion and biofilm development.[47] The GXM comprises >90% of the capsule's polysaccharide in addition to galactoxylomannan and mannoproteins.[48] Glycosyl composition analysis demonstrated a significant reduction in GXM sugar components, that is, glucuronic acid, xylose, and mannose (Figure 3C). The negative charge of cryptococcal cell capsule is by virtue of the glucuronic acid residues, and thus reduction in its content changes the cell surface charge. The reduction in the magnitude of negative charge obtained from the zeta potential (ZP) analysis substantiated the decrease in the capsule size (Figure 5).[49] Further, a significant decline in the rhamnose content of EPM was also observed (Figure 3C). Rhamnose is involved in adhesion and quorum sensing properties of cells in the biofilm.[50] Therefore, a decrease in the rhamnose content disrupts the biofilm EPM, leading to partial deactivation of the diffusion barrier. Henceforth, this course of events leads to a decrease in the EPM and cause biofilm inhibition (Figure 9; panel H).

DOI: 10.1021/acsomega.9b01482
ACS Omega 2019, 4, 17634−17648

4. CONCLUDING REMARKS

In summary, this is the first comprehensive report outlining the mode of action of small/amphipathic phenolic (THY/CARV) and aldehydic (CIT) terpenes against the *C. neoformans* biofilm. In general, all three terpenes followed a unified mechanism of action through multiple targets. However, the phenolic terpenes differed from aldehydic terpenes in their action at the level of cell membrane through selective sequestration of membrane ergosterol resulting in pore formation. At the intracellular level, both the group of terpenes mediated their action via a common mechanism including ergosterol biosynthesis inhibition, K^+/DNA/RNA efflux, ROS generation, and lipid peroxidation. In addition, oxidative stress caused reduction of the capsule size and EPM production, disrupting the structural and functional integrity of the *C. neoformans* biofilm. This study highlights the dual action of phenolic terpenes responsible for their more effectiveness in comparison to aldehydic terpenes. It also establishes a baseline for future studies focusing on the mode of action of these terpenes against different pathogenic biofilms. Moreover, the safety (as recognized by Food and Drug Administration, USA)[51] and efficacy of terpenes project these natural agents as a potential treatment option for device-associated biofilm infection. Furthermore, the structure of terpenes can act as a template for the development of novel therapeutic formulation against biofilms.

5. MATERIALS AND METHODS

5.1. Chemicals, Fungal Strain, and Growth Condition. Analytical grade THY (≥99%), CARV (≥99%), and CIT (≥95%) and standard antifungal drugs AMB, NYS, CASP, and FLC were purchased from Sigma-Aldrich, USA. A standard strain of *C. neoformans* (NCIM 3541 equivalent to ATCC 32045) isolated from an environmental source was procured from the National Collection of Industrial Microorganism, Pune. The strain was maintained on Sabouraud dextrose agar (HiMedia, India) at 4 °C. All experiments were carried out in conformity with Biosafety Level 2 (BSL-2) guidelines.

5.2. Biofilm Formation and Treatment Conditions. Biofilm formation was initiated by growing *C. neoformans* in Sabouraud dextrose broth (HiMedia, India) at 30 °C in an incubator shaker (150 rpm) for 24 h. After incubation, the pellet was centrifuged and washed thrice with sterile 1× phosphate-buffered saline (PBS pH 7, 0.1 M) to remove debris. The cells were then counted and resuspended at the density of 2×10^8 cells/mL in minimal medium (20 mg/mL thiamine, 30 mM glucose, 26 mM glycine, 20 mM $MgSO_4 \times 7H_2O$, and 58.8 mM KH_2PO_4). The suspension with a final density of 1×10^8 cells/mL in minimal media was added to fetal bovine serum (FBS, Gibco, United States)-pretreated 12-well culture plates, followed by static incubation for 24 h at 30 °C to form biofilms.[52] The BIC_{80} (lowest concentration of terpenes/drugs that cause 80% inhibition of the metabolic activity of biofilm formation) of terpenes/drugs were determined using the XTT reduction assay.[17] In the present study, sub-biofilm inhibitory concentration dosage (0.5× or 1/2 BIC_{80}) and time period of treatment (6 h after 24 h biofilm formation) were used to obtain substantial biomass for conducting various biophysical and biochemical assays and to analyze the response of biofilm cells against terpenes. These experimental conditions were considered on the basis of fungicidal kinetics of terpenes against *C. neoformans* (Figure S4).

5.3. Effect of Phenolic and Aldehydic Terpenes on the Surface Topography. *5.3.1. FE-SEM and AFM Analysis.* The 24 h biofilm formed on FBS-pretreated polystyrene discs in 12-well culture plates were subjected to treatment with 0.5× or 1/2 BIC_{80} of THY (16 μg/mL), CARV (32 μg/mL), and CIT (64 μg/mL) for another 6 h at 30 °C. The biofilm wells with 1% dimethyl sulfoxide (DMSO) in minimal medium and without terpenes served as CK (control). The CK and terpene-treated biofilms were then washed with sterile 1× PBS and fixed overnight with 2.5% glutaraldehyde. Following fixation, the biofilm was dehydrated in a series of ethanol solution (10−100%). For FE-SEM, the samples were dried, gold-sputtered, and visualized under the high-vacuum mode (15 kV) of a field emission scanning electron microscope (Quanta 200 FEG, USA). For the AFM analysis, the biofilm samples were air-dried followed by observation under an atomic force microscope (NT-MDT-INTEGRA, Ireland) in the contact mode with a reflex-coated silicon cantilever. The quantitative analysis related to cell height and surface roughness was done using automated NovaPX software integrated with the AFM instrument. The analysis was performed considering 4−5 images comprising 50 cells per treatment.

5.4. Estimation of Biomolecular Components in EPM after Terpene Treatment. *5.4.1. Isolation of EPM.* The preformed biofilm (24 h) on 12-well culture plates (FBS pretreated) was treated with THY (16 μg/mL), CARV (32 μg/mL), and CIT (64 μg/mL) for 6 h at 30 °C. The CK and terpene-treated biofilms were washed with sterile 1× PBS to remove nonadherent cells. The true biofilms were scraped from the bottom of the plate well with a sterilized micropipette tip and resuspended into Milli-Q water. For EPM isolation, the biofilm suspension was pooled and subjected to ultrasonication (Q700 sonicator, QSonica, Newtown, CT, USA) for 3 min @ 40 kHz.[53] The cell suspension was centrifuged (12 000 rpm) at 4 °C for 20 min, and the supernatant containing EPM was filtered through a 0.22 μm sterile syringe filter (Axiva, India). The separated pellet (biofilm cells) and EPM were analyzed (quantitative/qualitative) individually to assess the alternations in various biomolecules.

5.4.2. Qualitative and Quantitative Analyses of EPM. The CK and terpene-treated EPM samples were ethanol-precipitated and freeze-dried. Triple volumes of 100% cold ethanol were added to the EPM samples, followed by incubation in ice for 2 h. The precipitates formed were centrifuged (12 500 rpm, 20 min) at 4 °C and then freeze dried in a lyophilizer for overnight. For qualitative analysis, FT-IR spectroscopy (Thermo Nicolet NEXUS, USA) was performed for each sample (100 mg) at a range of 400−4000 cm^{-1} wavenumber. The samples were prepared using the potassium bromide-disk technique.

For the quantitative analysis, total carbohydrates and protein content in 100 mg sample of CK and terpene-treated EPM were determined. Polysaccharide content in the EPM was estimated by the phenol−sulphuric acid method[54] with glucose as the standard. The absorbance was measured at 485 nm using a spectrophotometer (Lasany, LI-2800 UV−visible double beam). The total protein content in the EPM was quantified by the Bradford method[55] using bovine serum albumin (BSA) as a standard followed by measurement at 592 nm in the microtiter plate reader (SpectraMax M2, Molecular Devices). The glycosyl composition of the EPM (CK and

DOI: 10.1021/acsomega.9b01482
ACS Omega 2019, 4, 17634−17648

terpene-treated) was quantitatively analyzed using gas chromatography−mass spectrometry (GC−MS).[56] Methyl glycosides were obtained by dissolving the dried samples (100 mg) in 100 μL of 20 mg/mL methoxyamine hydrochloride solution in pyridine (Sigma) and incubating the mixture at 75 °C for 30 min. The methyl glycosides samples were then trimethylsilylated (TMS) by adding 100 μL of *N*-methyl-*N*-trimethylsilyl trifluoroacetamide (Sigma) at 70 °C for 30 min. The analysis of the TMS methyl glycosides was performed using GC−MS (Agilent Technologies, USA) in a DB-5 capillary column (30 mm × 0.25 mm × 1 μm) with electron ionization of 70 eV and helium as the carrier gas at a flow rate of 1 mL/min. TMS methyl glycosides sample (1 μL) was injected at 250 °C in split mode (1:25). For analysis, the initial oven temperature was held at 70 °C for 2 min, ramped to 300 °C at a rate of 10 °C/min, and held for 5 min. TMS methyl glycosides were identified using the NIST 2005 database library.

5.5. Estimation of Biomolecular Components in Biofilm Cells. The cellular biofilm biomass of CK and terpene-treated samples obtained after EPM isolation was vacuum freeze-dried. Each biofilm cell sample (100 mg) was then grounded to get a homogeneous cell freeze-dried powder for the biomolecular composition (lipid, protein, and carbohydrate) analysis. FT-IR measurements were performed as described in Section 5.4.2.

Total lipids were isolated using the modified Bligh and Dyer method.[57] The total lipids were estimated gravimetrically, and the lipid content (%) was calculated by the following equation

$$\text{Lipid } \% = \frac{\text{total lipid (g)}}{\text{dry biomass (g)}} \times 100$$

The total nitrogen content in the lipid-extracted biofilm biomass was determined using a CHNS elemental analyzer (Thermo Scientific, USA). The total crude protein was evaluated using the following equation:[58]

$$\text{Protein } \% = \text{nitrogen content} \times 6.25$$

The total amount of carbohydrate in the lipid-extracted biofilm biomass was quantified using the phenol−sulphuric acid method with glucose as the standard.[54]

5.5.1. Fatty Acid Composition Analysis of Biofilm Cells. The 24 h biofilm was treated with THY (8, 16, and 32 μg/mL), CAR (16, 32, and 64 μg/mL), and CIT (32, 64, and 128 μg/mL) at their respective 0.25× or 1/4 BIC_{80}, 0.5× or 1/2 BIC_{80}, and 1× BIC_{80} for 6 h at 30 °C. The CK and terpene-treated biofilm cells were washed to remove nonattached cells, and the resultant true biofilm was scraped. The collected biofilm samples (100 mg) were subjected to total lipid extraction followed by trans-esterification into fatty acid methyl esters (FAMEs) by treatment of extracted lipids with methanolic sulphuric acid (6%) at 90 °C for 1 h. Further, hexane and distilled water (2:1 v/v) were added to the suspension and centrifuged at 5000 rpm for 5 min. The hexane containing FAMEs were then analyzed using GC−MS using a DB-5 capillary column. The FAME sample (1 μL) was injected at 250 °C in the split-less mode. The oven temperature was sequentially increased from the initial 50 to 180 °C and finally to 250 °C for 3 min.[58] The FAMEs were identified and quantified by analyzing their retention times in search against the NIST library. The data were expressed as a relative percentage of each fatty acid to the total fatty acid area.

5.6. Effect of Terpenes on the Cell Wall and Capsule. *5.6.1. Sorbitol Protection Assay.* Sorbitol assay was performed for planktonic cells and biofilm cells using the broth microdilution method and the biofilm formation assay in 96-well plates, as described previously with modifications.[17] For planktonic and biofilm cells, duplicate plates with wells containing the cell suspension (1−5 × 10^4 cells/mL and 2 × 10^8 cells/mL) in respective yeast nitrogen base (YNB) and minimal medium plus serially double diluted concentration of terpenes/CASP (2−1024 μg/mL) were prepared. The wells with 1% DMSO in YNB (planktonic cells) and minimal medium (biofilm cells) but without terpenes/drugs served as CK (control). One plate in the presence of sorbitol (0.8 M) and the other in the absence of sorbitol were incubated at 30 °C for 48 h and 7 days.[59] After incubation, MIC_{80} (lowest concentration of terpenes/drugs that cause 80% reduction of cell growth) for planktonic cells was determined by measuring absorbance at 530 nm, while BIC_{80} was determined by the colorimetric XTT reduction assay following measurement at 492 nm using a microtiter plate reader (SpectraMax, Molecular Devices, USA).

5.6.2. Capsule Size and Surface Charge Analysis. The formed biofilms (24 h) were treated at 0.5× or 1/2 BIC_{80} of THY (16 μg/mL), CARV (32 μg/mL), and CIT (64 μg/mL) for 6 h at 30 °C. The CK and terpene-treated biofilm samples were washed, scraped, and collected after centrifugation. The biofilm cells at a density of 10^4 cells/mL were resuspended in PBS, and a drop of Indian ink was added to each sample. The CK and terpene-treated samples were spread on slides followed by visualization under an optical microscope 100× (Axioplan; Carl Zeiss, Germany) for capsule measurement. Capsule size was measured as the difference between the cell wall and the outermost edge of the capsule. The measurements were performed by counting the capsule size of ∼50 cells using ImageJ software (National Institutes of Health, NIH, United States).[60] The surface charge on the CK and terpene-treated biofilm cells were estimated in suspension using a zeta sizer under 80 mV applied electric field at 25 °C (Malvern Zetasizer Nano Z-590 equipment). ZP values were calculated using Malvern software (version 7.03) as the average of 10 independent measurements, each obtained as the mean of 30 cell counts.[61]

5.7. Effect of Terpenes on Membrane Permeability and Integrity. *5.7.1. Ergosterol-Binding Assay.* The binding of terpenes to membrane ergosterol of *C. neoformans* planktonic and biofilm cells was assessed using the method described previously by Escalante et al. with minor modifications.[62] The duplicate 96-well plates for planktonic and biofilm cells were prepared as described above (in Section 5.6.1) with (2−1024 μg/mL) terpenes/positive control (AMB and NYS) in YNB and minimal medium, respectively. One plate from each duplicate plate for planktonic and biofilm cells was incubated in the absence and the other in the presence of exogenous ergosterol (100, 200, and 400 μg/mL) at 30 °C for 48 h. The MIC_{80} and BIC_{80} were determined as described above in Section 5.6.1.

5.7.2. Ergosterol Quantification Assay. The total intracellular ergosterol amount in 24 h formed biofilm after 6 h of treatment in the absence and presence of 0.25× or 1/4 BIC_{80}, 0.5× or 1/2 BIC_{80}, and 1× BIC_{80} of THY (8, 16, and 32 μg/mL), CARV (16, 32, and 64 μg/mL), and CIT (32, 64, and 128 μg/mL) with FLC (32, 64, and 128 μg/mL) as the positive control at 30 °C was quantified by adopting the

DOI: 10.1021/acsomega.9b01482
ACS Omega 2019, 4, 17634−17648

method of Khan et al.[63] Absorbances at 230 and 281.5 nm were recorded for detection of the 24(28) DHE (dehydroergosterol), an intermediary of the ergosterol pathway and ergosterol in the organic phase, respectively. The ergosterol content was estimated as a percentage of the wet weight of the cell pellet (100 mg) by the following equations

$$\%\ \text{ergosterol} = \frac{\left[\left\{\frac{A_{281.5}}{290}\right\} \times F\right]}{\text{pellet wt}} - \frac{\left[\left\{\frac{A_{230}}{518}\right\} \times F\right]}{\text{pellet wt}}$$

where F is the ethanol dilution factor and E is the molar extinction coefficient value of 290 and 518 determined in terms of % per cm for crystalline ergosterol and 24(28) DHE, respectively.[64]

5.7.3. Extracellular Potassium Leakage Assay. Extracellular K^+ leakage from the biofilm cells was estimated as described by Watanabe et al., with slight modifications.[65] Briefly, the 24 h biofilm cultured in minimal media was washed with 1× PBS to remove nonadherent cells. The resultant true biofilm was scraped, and the cells were collected by centrifugation (4000 rpm, 5 min) followed by washing with deionized water. The cells were resuspended at a concentration of 5×10^4 biofilm cells/mL in deionized water, and 1 mL of this suspension was incubated with 1/2 BIC_{80} concentration of THY (16 μg/mL), CARV (32 μg/mL), and CIT (64 μg/mL) for 2, 4, 6, and 8 h at 30 °C. *C. neoformans* biofilm cells incubated with deionized water only was used as CK. After treatment, the samples were collected by centrifugation (10 000 rpm) for 10 min, and the supernatant was stored for the estimation of extracellular K^+ content released into the deionized water. The K^+ concentration was determined using inductively coupled plasma mass spectrometer (PerkinElmer, USA).

5.7.4. Intracellular Content and Protein Release. The biofilm formed in minimal media at 30 °C for 24 h was scraped, washed, and resuspended in phosphate buffer (0.1 M, pH 7.5). Two sets of four microcentrifuge tubes, each containing an inoculum of 5×10^4 biofilm cells/mL without and with 0.5× or 1/2 BIC_{80} concentrations of THY (16 μg/mL), CARV (32 μg/mL), and CIT (64 μg/mL) were incubated at 30 °C for a series of time intervals ranging from 0 to 8 h. After incubation, the cell suspension was centrifuged (10 min at 10 000 rpm) and the supernatants (100 μL) were collected. The absorbance of one set of supernatant was measured at 260 nm and the other set at 280 nm using an ultraviolet−visible (UV−vis) spectrophotometer to estimate the release of intracellular content (DNA/RNA/Nucleotides) and protein, respectively.[66]

5.7.5. Plasma Membrane Integrity Assay. The 24 h biofilms after treatment with 0.5× or 1/2 BIC_{80} of THY (16 μg/mL), CARV (32 μg/mL), CIT (64 μg/mL), and AMB (2 μg/mL) as a positive control for 6 h at 30 °C were washed with PBS and collected. The CK and treated biofilm cells (10^6 cells/mL) were resuspended in PBS and transferred into microcentrifuge tubes. Then, 1 mg/mL PI (Sigma-Aldrich) dye was added to each of the above tubes and incubated in the dark (30 min) at 37 °C. After incubation, the cells were washed twice with 1× PBS to eliminate the excess dye, and the fluorescence was measured using a fluorometer (Fluorolog-3 LS55, Horiba Jobin Yvon Spex, Edison, NJ, USA) with the excitation and emission wavelengths of 535 and 617 nm, respectively, and the images were captured using a fluorescence microscope (Axioplan; Carl Zeiss, Germany).[67]

5.8. Oxidative Stress and Antioxidant Defense System Responses after Terpene Treatment. The 24 h biofilm was treated with 0.5× or 1/2 BIC_{80} of THY (16 μg/mL), CARV (32 μg/mL), and CIT (64 μg/mL) and 5 mM HP (positive control) for 6 h at 30 °C.

5.8.1. Assessment of Mitochondrial Membrane Potential. The effect of terpenes on the mitochondrial membrane potential ($\Delta\psi_m$) was measured using fluorescent probes Rho123. The CK and terpene-treated biofilm cells at the density of 10^6 cells/mL were collected and washed with PBS followed by incubation in Rho123 (50 μM) for 30 min at 37 °C. After incubation, the cells were washed twice with PBS to remove the excess staining and further resuspended in PBS. The fluorescence intensity was measured using a fluorometer with the excitation and emission wavelengths of 505 and 534 nm, respectively. Additionally, the Rho123-stained cells were observed, and the images were captured under a fluorescent microscope.

5.8.2. ROS Quantification and Lipid Peroxidation. For endogenous ROS quantification, 10 μM of the fluorescent probe, 2′,7′-dichlorofluorescein diacetate (H2DCFDA; Sigma-Aldrich), was added to CK and terpene-treated biofilm wells (10^6 cells/mL) in 12-well culture plates. The plates were incubated at 30 °C for 30 min in the dark. After incubation, the biofilm samples were washed with 1× PBS to reduce background fluorescence. The fluorescence intensity was measured using a fluorometer with excitation and emission wavelengths of 495 and 525 nm.[67] Further, the DCFDA-stained cells were observed under a fluorescence microscope and images were captured.

For lipid peroxidation, the CK and terpene-treated biofilm cell pellet (100 mg) was frozen and homogenized with 1 mL of chilled phosphoric acid (1.1%). The homogenate was mixed in the ratio 1:1 with 1% thiobarbituric acid (TBA, Sigma-Aldrich, United States) in NaOH.[68] The above samples were heated at 98 °C (1 h) followed by the addition of a double volume of butanol, and finally the mixture was centrifuged at 4000 rpm (5 min). The absorbance of the organic layer was measured in a quartz cuvette with a path length 1 cm at 532 nm corrected for nonspecific turbidity due to TBA abduct at 600 nm. Lipid peroxidation products, TBARS content were measured using the following formula

$$\text{TBARS content} = (A_{532} - A_{600})/\text{EC}$$

where A is the absorbance in nm and EC is the extinction coefficient (156 mM^{-1} cm^{-1}).

5.8.3. SOD, CAT, and POD Activities. Cell-free extracts of CK and the terpene-treated biofilm (100 mg) were prepared as described previously by Khan et al., with little modifications.[69] Biofilm cells were disrupted by liquid nitrogen and then resuspended in 1 mL of grinding buffer (250 mM sucrose, 10 mM Tris-HCl, pH 7.5, 1 mM PMSF). The above homogenate was centrifuged at 15 000 rpm for 45 min at 4 °C. Soluble protein was estimated using the Bradford test with BSA as the standard. Enzyme activities were measured using a UV−vis spectrophotometer (Cary 5000 UV−vis−NIR, Agilent, USA).

The SOD activity was measured using the method previously described by Ferreira et al.[68] The cell-free extract (100 μL) and pyrogallol-tris buffer (100 μL) were mixed followed by observation of pyrogallol inhibition every 30 s for 3 min at 420 nm. The units of SOD were measured as pyrogallol autoxidation per 200 μL and calculated as follows

DOI: 10.1021/acsomega.9b01482
ACS Omega 2019, 4, 17634−17648

$$\frac{\text{Units of SOD}}{\text{mL}} = \left[\frac{(A-B)}{A} \times 50 \times 100\right] \times 0.6\ (\text{df})$$

where A is the difference in absorbance per 1 min in the control, B is the difference in absorbance per 1 min in the test samples, and df is the dilution factor. Results are expressed in U/mg protein.

For CAT activity, 10 μL of cell-free extract was added to 1.99 mL of phosphate buffer (0.05 M, pH 7.0) and 1.0 mL of H_2O_2 (0.0019 M) making a total volume of 3.0 mL as the reaction mixture. The fall in absorbance because of the disappearance of H_2O_2 was recorded for 30 s intervals up to 3 min in a quartz cuvette (path length = 1 cm) at 240 nm (25 °C). The CAT activity was evaluated in terms of μmol H_2O_2 consumed/min/mg protein using a molar extinction coefficient of 43.6 M^{-1} cm^{-1}.

For POD activity, 100 μL of the cell-free extract was added in 25 mM *N*-(2-hydroxyethyl)piperazine-*N*′-ethanesulfonic acid solution (pH 6.8, HiMedia, India) containing 10 mM H_2O_2 and 4 mM guaiacol (HiMedia, India) and incubated for 15 min. The change in absorbance due to tetraguaiacol formation was monitored every 30 s for 3 min of reaction in a quartz cuvette (path length = 1 cm) at 470 nm (25 °C). POD activity was expressed in μmol/min/mg protein using a molar extinction coefficient of 26.61 M^{-1} cm^{-1}.

5.9. Statistical Analysis. All experiments were carried out in triplicate. The data are represented as average ± standard deviation (SD). One-way analysis of variance followed by *t*-test was employed for analyzing the statistical significance between treated and control groups. Statistically significant differences were defined only when the *p*-value was less than 0.05 and are denoted by asterisks $*p < 0.05$, $**p < 0.01$, and $***p < 0.001$.

■ ASSOCIATED CONTENT

Supporting Information

The Supporting Information is available free of charge on the ACS Publications website at DOI: 10.1021/acsomega.9b01482.

Percentage of protein in the EPM of *C. neoformans* biofilm before and after phenolic/aldehydic terpene treatment at 1/2 BIC80 for 6 h, percentage of carbohydrates and proteins in biofilm cells of *C. neoformans* before and after phenolic/aldehydic terpene treatment for 6 h, logarithmic fungicidal kinetic curves of terpenes and standard drugs at respective 1/2 BIC80 against *C. neoformans in* comparison to CK, BIC80, 1/2 BIC80, and 1/4 BIC80 of terpenes and standard drugs against *C. neoformans*, and changes in the UFA/SFA ratio of total lipid composition of *C. neoformans* after treatment at different BIC80 of terpenes (PDF)

■ AUTHOR INFORMATION

Corresponding Authors

*E-mail: mohanpmk@gmail.com, krishfbt@iitr.ac.in. Phone: 091-1332-284779 (K.M.P.).

*E-mail: rapdyfbs@iitr.ac.in, girsh.chandra8@gmail.com. Phone: 091-1332-285791 (R.P.).

ORCID

Krishna Mohan Poluri: 0000-0003-3801-7134

Ramasare Prasad: 0000-0001-7341-2346

Notes

The authors declare no competing financial interest.

■ ACKNOWLEDGMENTS

P.K. acknowledges the receipt of financial support in the form of fellowship [grant no: 09/143(0857)/2014-EMR-I] from the Council of Scientific and Industrial Research, (CSIR), New Delhi, India. The authors thank the Institute Instrumentation Centre (IIC) for analytical and microscopic instrumentation support.

■ REFERENCES

(1) Rajasingham, R.; Smith, R. M.; Park, B. J.; Jarvis, J. N.; Govender, N. P.; Chiller, T. M.; Denning, D. W.; Loyse, A.; Boulware, D. R. Global burden of disease of HIV-associated cryptococcal meningitis: an updated analysis. *Lancet Infect. Dis.* **2017**, *17*, 873−881.

(2) Maziarz, E. K.; Perfect, J. R. Cryptococcosis. *Infect. Dis. Clin. North Am.* **2016**, *30*, 179−206.

(3) Aslanyan, L.; Sanchez, D.; Valdebenito, S.; Eugenin, E.; Ramos, R.; Martinez, L. The crucial role of biofilms in Cryptococcus neoformans survival within macrophages and colonization of the central nervous system. *J. Fungi* **2017**, *3*, 1−12.

(4) Foong, K. S.; Lee, A.; Vasquez, G. Cryptococcal Infection of the Ventriculoperitoneal Shunt in an Immunocompetent Patient. *Am. J. Case Rep.* **2016**, *17*, 31−34.

(5) Benaducci, T.; Sardi, J. C. O.; Lourencetti, N. M. S.; Scorzoni, L.; Gullo, F. P.; Rossi, S. A.; Derissi, J. B.; Prata, M. C. A.; Fusco-Almeida, A. M.; Mendes-Giannini, M. J. S. Virulence of Cryptococcus sp. Biofilms In Vitro and In Vivo using Galleria mellonella as an Alternative Model. *Front. Microbiol.* **2016**, *7*, 290.

(6) Flemming, H.-C.; Wingender, J. The Biofilm Matrix. *Nat. Rev. Microbiol.* **2010**, *8*, 623−633.

(7) Martinez, L. R.; Casadevall, A. Specific antibody can prevent fungal biofilm formation and this effect correlates with protective efficacy. *Infect. Immun.* **2005**, *73*, 6350−6362.

(8) Zaragoza, O.; Rodrigues, M. L.; De Jesus, M.; Frases, S.; Dadachova, E.; Casadevall, A. The capsule of the fungal pathogen Cryptococcus neoformans. *Adv. Appl. Microbiol.* **2009**, *68*, 133−216.

(9) May, R. C.; Stone, N. R. H.; Wiesner, D. L.; Bicanic, T.; Nielsen, K. Cryptococcus: from environmental saprophyte to global pathogen. *Nat. Rev. Microbiol.* **2016**, *14*, 106−117.

(10) Delattin, N.; Cammue, B. P.; Thevissen, K. Reactive oxygen species-inducing antifungal agents and their activity against fungal biofilms. *Future Med. Chem.* **2014**, *6*, 77−90.

(11) Martinez, L. R.; Casadevall, A. Susceptibility of Cryptococcus neoformans biofilms to antifungal agents in vitro. *Antimicrob. Agents Chemother.* **2006**, *50*, 1021−1033.

(12) Nett, J. E.; Sanchez, H.; Cain, M. T.; Andes, D. R. Genetic Basis ofCandidaBiofilm Resistance Due to Drug-Sequestering Matrix Glucan. *J. Infect. Dis.* **2010**, *202*, 171−175.

(13) Nett, J. E.; Andes, D. Fungal Biofilms: In vivo models for discovery of anti-biofilm drugs. *Microbiol. Spectrum* **2015**, *3*, 1−25.

(14) Abbaszadeh, S.; Sharifzadeh, A.; Shokri, H.; Khosravi, A. R.; Abbaszadeh, A. Antifungal efficacy of thymol, carvacrol, eugenol and menthol as alternative agents to control the growth of food-relevant fungi. *J. Mycol. Med.* **2014**, *24*, e51−e56.

(15) Chatrath, A.; Gangwar, R.; Kumari, P.; Prasad, R. In vitro anti-biofilm activities of citral and thymol against Candida tropicalis. *J. Fungi* **2019**, *5*, 13.

(16) Raei, P.; Pourlak, T.; Memar, M. Y.; Alizadeh, N.; Aghamali, M.; Zeinalzadeh, E.; Asgharzadeh, M.; Kafil, H. S. Thymol and carvacrol strongly inhibit biofilm formation and growth of carbapenemase-producing gram negative bacilli. *Cell. Mol. Biol.* **2017**, *63*, 108−112.

(17) Kumari, P.; Mishra, R.; Arora, N.; Chatrath, A.; Gangwar, R.; Roy, P.; Prasad, R. Antifungal and anti-biofilm activity of essential oil active components against Cryptococcus neoformans and Cryptococcus laurentii. *Front. Microbiol.* **2017**, *8*, 2161.

(18) Lambert, R. J. W.; Skandamis, P. N.; Coote, P. J.; Nychas, G.-J. E. A study of the minimum inhibitory concentration and mode of

DOI: 10.1021/acsomega.9b01482
ACS Omega 2019, 4, 17634−17648

action of oregano essential oil, thymol and carvacrol. *J. Appl. Microbiol.* **2001**, *91*, 453−462.
(19) Leite, M. C. A.; Bezerra, A. P. d. B.; de Sousa, J. P.; Guerra, F. Q. S.; Lima, E. d. O. Evaluation of antifungal activity and mechanism of action of citral against Candida albicans. *Evid. Based Complement Altern. Med.* **2014**, *11*, 1−9.
(20) Tyagi, A. K.; Malik, A. Liquid and vapour-phase antifungal activities of selected essential oils against Candida albicans: microscopic observations and chemical characterization of Cymbopogon citratus. *BMC Complementary Altern. Med.* **2010**, *10*, 65.
(21) Maquelin, K.; Kirschner, C.; Choo-Smith, L.-P.; van den Braak, N.; Endtz, H. P.; Naumann, D.; Puppels, G. J. Identification of medically relevant microorganisms by vibrational spectroscopy. *J. Microbiol. Methods* **2002**, *51*, 255−271.
(22) Mester, P.; Jehle, A. K.; Leeb, C.; Kalb, R.; Grunert, T.; Rossmanith, P. FTIR metabolomic fingerprint reveals different modes of action exerted by active pharmaceutical ingredient based ionic liquids (API-ILS) on Salmonella typhimurium. *RSC Adv.* **2016**, *6*, 32220−32227.
(23) Di Pasqua, R.; Hoskins, N.; Betts, G.; Mauriello, G. Changes in membrane fatty acids composition of microbial cells induced by addiction of thymol, carvacrol, limonene, cinnamaldehyde, and eugenol in the growing media. *J. Agric. Food Chem.* **2006**, *54*, 2745−2749.
(24) Lupetti, A.; Danesi, R.; Campa, M.; Del Tacca, M.; Kelly, S. Molecular basis of resistance to azole antifungals. *Trends Mol. Med.* **2002**, *8*, 76−81.
(25) Ott, M.; Gogvadze, V.; Orrenius, S.; Zhivotovsky, B. Mitochondria, oxidative stress and cell death. *Apoptosis* **2007**, *12*, 913−922.
(26) Ramage, G.; Rajendran, R.; Sherry, L.; Williams, C. Fungal biofilm resistance. *Internet J. Microbiol.* **2012**, *2012*, 1−14.
(27) Nett, J. E.; Crawford, K.; Marchillo, K.; Andes, D. R. Role of Fks1p and matrix glucan in Candida albicans biofilm resistance to an echinocandin, pyrimidine, and polyene. *Antimicrob. Agents Chemother.* **2010**, *54*, 3505−3508.
(28) Samaranayake, Y. H.; Ye, J.; Yau, J. Y. Y.; Cheung, B. P. K.; Samaranayake, L. P. In vitro method to study antifungal perfusion in Candida biofilms. *J. Clin. Microbiol.* **2005**, *43*, 818−825.
(29) Mitchell, K. F.; Zarnowski, R.; Andes, D. R. Fungal super glue: The biofilm matrix and its composition, assembly, and functions. *PLoS Pathog.* **2016**, *12*, No. e1005828.
(30) Elshafie, H.; Armentano, M.; Carmosino, M.; Bufo, S.; De Feo, V.; Camele, I. Cytotoxic activity of Origanum vulgare L. on hepatocellular carcinoma cell line HepG2 and evaluation of its biological activity. *Molecules* **2017**, *22*, 1435.
(31) Ferreira, J. V. N.; Capello, T. M.; Siqueira, L. J. A.; Lago, J. H. G.; Caseli, L. Mechanism of Action of Thymol on Cell Membranes Investigated through Lipid Langmuir Monolayers at the Air-Water Interface and Molecular Simulation. *Langmuir* **2016**, *32*, 3234−3241.
(32) Sousa, J.; Costa, A.; Leite, M.; Guerra, F.; Silva, V.; Menezes, C.; Pereira, F.; Lima, E. Antifungal activity of citral by disruption of ergosterol biosynthesis in fluconazole resistant Candida tropicalis. *Int. J. Trop. Dis.* **2016**, *11*, 1−11.
(33) Wang, Y.; Feng, K.; Yang, H.; Yuan, Y.; Yue, T. Antifungal mechanism of cinnamaldehyde and citral combination against Penicillium expansum based on FT-IR fingerprint, plasma membrane, oxidative stress and volatile profile. *RSC Adv.* **2018**, *8*, 5806−5815.
(34) Ahmad, A.; Khan, A.; Akhtar, F.; Yousuf, S.; Xess, I.; Khan, L. A.; Manzoor, N. Fungicidal activity of thymol and carvacrol by disrupting ergosterol biosynthesis and membrane integrity against Candida. *Eur. J. Clin. Microbiol. Infect. Dis.* **2011**, *30*, 41−50.
(35) Siroli, L.; Patrignani, F.; Gardini, F.; Lanciotti, R. Effects of sublethal concentrations of thyme and oregano essential oils, carvacrol, thymol, citral and trans-2-hexenal on membrane fatty acid composition and volatile molecule profile of Listeria monocytogenes, Escherichia coli and Salmonella enteritidis. *Food Chem.* **2015**, *182*, 185−192.
(36) Leekumjorn, S.; Cho, H. J.; Wu, Y.; Wright, N. T.; Sum, A. K.; Chan, C. The role of fatty acid unsaturation in minimizing biophysical changes on the structure and local effects of bilayer membranes. *Biochim. Biophys. Acta* **2009**, *1788*, 1508−1516.
(37) Lyu, F.; Gao, F.; Wei, Q.; Liu, L. Changes of membrane fatty acids and proteins of Shewanella putrefaciens treated with cinnamon oil and gamma irradiation. *Bioresour. Bioprocess.* **2017**, *4*, 1−10.
(38) Chekem, M. S. G.; Lunga, P. K.; Tamokou, J. D. D.; Kuiate, J. R.; Tane, P.; Vilarem, G.; Cerny, M. Antifungal properties of Chenopodium ambrosioides essential oil against Candida species. *Pharmaceuticals* **2010**, *3*, 2900−2909.
(39) Hu, L.-B.; Ban, F.-F.; Li, H.-B.; Qian, P.-P.; Shen, Q.-S.; Zhao, Y.-Y.; Mo, H.-Z.; Zhou, X. Thymol Induces Conidial Apoptosis in Aspergillus flavus via Stimulating K+ Eruption. *J. Agric. Food Chem.* **2018**, *66*, 8530−8536.
(40) Kim, J. H.; Lee, H.-O.; Cho, Y.-J.; Kim, J.; Chun, J.; Choi, J.; Lee, Y.; Jung, W. H. A vanillin derivative causes mitochondrial dysfunction and triggers oxidative stress in Cryptococcus neoformans. *PLoS One* **2014**, *9*, No. e89122.
(41) Khan, I.; Bahuguna, A.; Kumar, P.; Bajpai, V. K.; Kang, S. C. Antimicrobial potential of carvacrol against uropathogenic Escherichia coli via membrane disruption, depolarization, and reactive oxygen species generation. *Front. Microbiol.* **2017**, *8*, 2421.
(42) OuYang, Q.; Tao, N.; Zhang, M. A Damaged oxidative phosphorylation mechanism is involved in the antifungal activity of citral against Penicillium digitatum. *Front. Microbiol.* **2018**, *9*, 239.
(43) Li, Y.; Shao, X.; Xu, J.; Wei, Y.; Xu, F.; Wang, H. Tea tree oil exhibits antifungal activity against Botrytis cinerea by affecting mitochondria. *Food Chem.* **2017**, *234*, 62−67.
(44) Alves, J. C. O.; Ferreira, G. F.; Santos, J. R.; Silva, L. C. N.; Rodrigues, J. F. S.; Neto, W. R. N.; Farah, E. I.; Santos, Á. R. C.; Mendes, B. S.; Sousa, L. V. N. F.; Monteiro, A. S.; dos Santos, V. L.; Santos, D. A.; Perez, A. C.; Romero, T. R. L.; Denadai, A. M. L.; Guzzo, L. S. Eugenol induces phenotypic alterations and increases the oxidative burst in Cryptococcus. *Front. Microbiol.* **2017**, *8*, 2419.
(45) Trevijano-Contador, N.; Rossi, S. A.; Alves, E.; Landin-Ferreiroa, S.; Zaragoza, O. Capsule enlargement in Cryptococcus neoformans is dependent on mitochondrial activity. *Front. Microbiol.* **2017**, *8*, 1423.
(46) Panariello, B. H. D.; Klein, M. I.; Mima, E. G. D. O.; Pavarina, A. C. Fluconazole impacts the extracellular matrix of fluconazole-susceptible and -resistant Candida albicans and Candida glabrata biofilms. *J. Oral Microbiol.* **2018**, *10*, 1476644.
(47) Martinez, L. R.; Casadevall, A. Cryptococcus neoformans biofilm formation depends on surface support and carbon source and reduces fungal cell susceptibility to heat, cold, and UV light. *Appl. Environ. Microbiol.* **2007**, *73*, 4592−4601.
(48) Wang, Z. A.; Li, L. X.; Doering, T. L. Unraveling synthesis of the cryptococcal cell wall and capsule. *Glycobiology* **2018**, *28*, 719−730.
(49) Nosanchuk, J. D.; Casadevall, A. Cellular charge of Cryptococcus neoformans: contributions from the capsular polysaccharide, melanin, and monoclonal antibody binding. *Infect. Immun.* **1997**, *65*, 1836−1841.
(50) Mongkolrob, R.; Taweechaisupapong, S.; Tungpradabkul, S. Correlation between biofilm production, antibiotic susceptibility and exopolysaccharide composition inBurkholderia pseudomalleibpsI,ppk, andrpoS mutant strains. *Microbiol. Immunol.* **2015**, *59*, 653−663.
(51) Ramos, M.; Beltran, A.; Valdes, A.; Peltzer, M. A.; Jimenez, A.; Garrigos, M. C.; Zaikov, G. E. Carvacrol and Thymol for Fresh Food Packaging. *J. Bioequivalence Bioavailability* **2013**, *5*, 154.
(52) Pettit, R. K.; Repp, K. K.; Hazen, K. C. Temperature affects the susceptibility ofCryptococcus neoformansbiofilms to antifungal agents. *Med. Mycol.* **2010**, *48*, 421−426.
(53) Ajesh, K.; Sreejith, K. Cryptococcus laurentii Biofilms: Structure, Development and Antifungal Drug Resistance. *Mycopathologia* **2012**, *174*, 409−419.

DOI: 10.1021/acsomega.9b01482
ACS Omega 2019, 4, 17634−17648

(54) Dubois, M.; Gilles, K. A.; Hamilton, J. K.; Rebers, P. A.; Smith, F. Colorimetric method for determination of sugars and related substances. *Anal. Chem.* **1956**, *28*, 350−356.
(55) Bradford, M. M. A rapid and sensitive method for the quantitation of microgram quantities of protein utilizing the principle of protein-dye binding. *Anal. Biochem.* **1976**, *72*, 248−254.
(56) Lisec, J.; Schauer, N.; Kopka, J.; Willmitzer, L.; Fernie, A. R. Gas chromatography mass spectrometry-based metabolite profiling in plants. *Nat. Protoc.* **2015**, *1*, 387−396.
(57) Arora, N.; Patel, A.; Pruthi, P. A.; Pruthi, V. Boosting TAG accumulation with improved biodiesel production from novel oleaginous microalgae Scenedesmus sp. IITRIND2 utilizing waste sugarcane bagasse aqueous extract (SBAE). *Appl. Biochem. Biotechnol.* **2016**, *180*, 109−121.
(58) Arora, N.; Patel, A.; Pruthi, P. A.; Pruthi, V. Synergistic dynamics of nitrogen and phosphorous influences lipid productivity in Chlorella minutissima for biodiesel production. *Bioresour. Technol.* **2016**, *213*, 79−87.
(59) de Castro, R. D.; de Souza, T. M. P. A.; Bezerra, L. M. D.; Ferreira, G. L. S.; Costa, E. M. M. d. B.; Cavalcanti, A. L. Antifungal activity and mode of action of thymol and its synergism with nystatin against Candida species involved with infections in the oral cavity: an in vitro study. *BMC Complementary Altern. Med.* **2015**, *15*, 417.
(60) Araujo, G. d. S.; Fonseca, F. L.; Pontes, B.; Torres, A.; Cordero, R. J. B.; Zancopé-Oliveira, R. M.; Casadevall, A.; Viana, N. B.; Nimrichter, L.; Rodrigues, M. L.; Garcia, E. S.; de Souza, W.; Frases, S. Capsules from pathogenic and non-pathogenic Cryptococcus spp. manifest significant differences in structure and ability to protect against phagocytic cells. *PLoS One* **2012**, *7*, No. e29561.
(61) Nosanchuk, J. D.; Cleare, W.; Franzot, S. P.; Casadevall, A. Amphotericin B and fluconazole affect cellular charge, macrophage phagocytosis, and cellular morphology of Cryptococcus neoformans at subinhibitory concentrations. *Antimicrob. Agents Chemother.* **1999**, *43*, 233−239.
(62) Escalante, A.; Gattuso, M.; Pérez, P.; Zacchino, S. Evidence for the Mechanism of Action of the Antifungal Phytolaccoside B Isolated fromPhytolacca tetrameraHauman. *J. Nat. Prod.* **2008**, *71*, 1720−1725.
(63) Khan, M. S.; Ahmad, I.; Cameotra, S. Phenyl aldehyde and propanoids exert multiple sites of action towards cell membrane and cell wall targeting ergosterol in Candida albicans. *AMB Express* **2013**, *3*, 54.
(64) Singh, S.; Fatima, Z.; Hameed, S. Citronellal-induced disruption of membrane homeostasis in Candida albicans and attenuation of its virulence attributes. *Rev Soc Bras Med Trop* **2016**, *49*, 465−472.
(65) Watanabe, H.; Azuma, M.; Igarashi, K.; Ooshima, H. Relationship between cell morphology and intracellular potassium concentration in Candida albicans. *J. Antibiot.* **2006**, *59*, 281−287.
(66) Miksusanti; Jenie, B. S. L.; Priosoeryanto, B. P.; Syarief, R.; Rekso, G. T. Mode of Action Temu Kunci (Kaempferia pandurata) Essential Oil on E. coli K1.1 Cell Determined by Leakage of Material Cell and Salt Tolerance Assays. *HAYATI J. Biosci.* **2008**, *15*, 56−60.
(67) Pemmaraju, S. C.; Padmapriya, K.; Pruthi, P. A.; Prasad, R.; Pruthi, V. Impact of oxidative and osmotic stresses onCandida albicansbiofilm formation. *Biofouling* **2016**, *32*, 897−909.
(68) Ferreira, G. F.; Baltazar, L. d. M.; Santos, J. R. A.; Monteiro, A. S.; Fraga, L. A. d. O.; Resende-Stoianoff, M. A.; Santos, D. A. The role of oxidative and nitrosative bursts caused by azoles and amphotericin b against the fungal pathogen Cryptococcus gattii. *J. Antimicrob. Chemother.* **2013**, *68*, 1801−1811.
(69) Khan, A.; Ahmad, A.; Akhtar, F.; Yousuf, S.; Xess, I.; Khan, L. A.; Manzoor, N. Induction of oxidative stress as a possible mechanism of the antifungal action of three phenylpropanoids. *FEMS Yeast Res.* **2011**, *11*, 114−122.

DOI: 10.1021/acsomega.9b01482
ACS Omega 2019, 4, 17634−17648